Biochemical Pharmacology 150 (2018) 86–96

Contents lists available at ScienceDirect

Biochemical Pharmacology

journal homepage: www.elsevier.com/locate/biochempharm

Activation of mitochondrial fusion provides a new treatment for mitochondria-related diseases

Aliz Szabo[a], Katalin Sumegi[a], Katalin Fekete[a], Eniko Hocsak[a], Balazs Debreceni[a], Gyorgy Setalo Jr.[b,c], Krisztina Kovacs[a], Laszlo Deres[c,d], Andras Kengyel[e], Dominika Kovacs[a], Jozsef Mandl[f], Miklos Nyitrai[e], Mark A. Febbraio[g], Ferenc Gallyas Jr.[a,c,h], Balazs Sumegi[a,c,h,*]

[a] Department of Biochemistry and Medical Chemistry, University of Pécs Medical School, Pécs, Hungary
[b] Department of Medical Biology, University of Pécs Medical School, Pécs, Hungary
[c] Szentagothai Research Centre, University of Pécs, Pécs, Hungary
[d] 1st Department of Medicine, Division of Cardiology, University of Pecs Medical School, Pecs, Hungary
[e] Department of Biophysics, University of Pécs Medical School, Pécs, Hungary
[f] Department of Medical Chemistry, Molecular Biology and Pathobiochemistry, Semmelweis University, Budapest, Hungary
[g] Cellular and Molecular Metabolism Laboratory, Garvan Institute of Medical Research, Darlinghurst, Sydney, Australia
[h] Nuclear-Mitochondrial Interactions Research Group, Hungarian Academy of Sciences, Budapest, Hungary

ARTICLE INFO

Keywords:
Mitochondrial fragmentation
BGP-15
Oxidative stress
Optic atrophy 1

ABSTRACT

Mitochondria fragmentation destabilizes mitochondrial membranes, promotes oxidative stress and facilitates cell death, thereby contributing to the development and the progression of several mitochondria-related diseases. Accordingly, compounds that reverse mitochondrial fragmentation could have therapeutic potential in treating such diseases. BGP-15, a hydroxylamine derivative, prevents insulin resistance in humans and protects against several oxidative stress-related diseases in animal models. Here we show that BGP-15 promotes mitochondrial fusion by activating optic atrophy 1 (OPA1), a GTPase dynamin protein that assist fusion of the inner mitochondrial membranes. Suppression of Mfn1, Mfn2 or OPA1 prevents BGP-15-induced mitochondrial fusion. BGP-15 activates Akt, S6K, mTOR, ERK1/2 and AS160, and reduces JNK phosphorylation which can contribute to its protective effects. Furthermore, BGP-15 protects lung structure, activates mitochondrial fusion, and stabilizes cristae membranes *in vivo* determined by electron microscopy in a model of pulmonary arterial hypertension. These data provide the first evidence that a drug promoting mitochondrial fusion in *in vitro* and *in vivo* systems can reduce or prevent the progression of mitochondria-related disorders.

1. Introduction

Mitochondria are the major energy-producing organelles, and play a significant role in determining cell survival and death [1–4]. They are dynamic organelles undergoing frequent fission and fusion cycles that result in major morphological changes. Membrane bound dynamin GTPases, dynamin-related protein 1 (Drp1), mitochondrial fission protein 1 (Fis1), mitofusin 1/2 (Mfn1/2) and optic atrophy 1 (OPA1) drive these changes [5–7]. Mitochondrial fragmentation plays an important role in the development and progression of several diseases, including diabetes [4,8–12], neurodegenerative diseases [5,13,14], muscular dystrophies [15,16], nonalcoholic fatty liver disease and other types of hepatotoxicity [17–19], and pulmonary arterial hypertension (PAH) [20,21] and several other diseases related to oxidative stress [2,22].

Reactive oxygen species (ROS) deriving from different sources induce activated mitochondrial fission catalyzed by Drp1 and Fis1, and lead to fragmented mitochondria [1–4,8]. These mitochondria have lower membrane potential, produce less ATP, generate significantly more ROS, and facilitate the release of proapoptotic mitochondrial proteins [7,16,23]. Therefore, modulation of mitochondrial fission or fusion pathways by synthetic chemicals could provide novel molecular mechanism to protect cells in oxidative stress, and could be a new way to design novel mitochondrial drugs.

BGP-15 (O-[3-piperidino-2-hydroxy-1-propyl]-nicotinic amidoxime) possesses a wide range of cytoprotective effects [24–33] but lacks a clear intracellular molecular target. BGP-15 protects the mitochondrial membrane system, decreases oxidative stress [27,28], inhibits the nuclear translocation of apoptosis-inducing factor (AIF) from mitochondria [27], and inhibits mitogen-activated protein kinase (MAPK) activation [26,29]. BGP-15 is effective in ameliorating obesity induced

* Corresponding author at: Department of Biochemistry and Medical Chemistry, University of Pécs, Szigeti út 12, H-7624 Pécs, Hungary.
E-mail address: balazs.sumegi@aok.pte.hu (B. Sumegi).

https://doi.org/10.1016/j.bcp.2018.01.038
Received 4 December 2017; Accepted 22 January 2018

insulin resistance [29,33], improves insulin action in humans [30], slows the progression of severe muscular dystrophy [24], and also increases mitochondrial biogenesis [33] in rodents.

Based on the observations above, we raise the possibility that BGP-15 can influence mitochondrial fragmentation, and provide evidence in cultured cells that BGP-15-activated mitochondrial fusion requires active OPA1, Mfn1/2 and Akt (also called protein kinase B). In addition, we show that BGP-15 activates OPA1 GTPase and promotes its polymerization *in vitro*. Since oxidative stress and mitochondrial fragmentation play important role in the development of PAH [20,21], we used this model to provide evidence for the BGP-15-induced mitochondrial fusion in an *in vivo* system.

2. Materials and methods

2.1. Materials

All chemicals for cell culture studies were from PAA Laboratories (Cölbe, Germany) and Gibco/Invitrogen (Life Technologies, Carlsbad, CA, USA). Hydrogen peroxide (H_2O_2), protease inhibitor mixture and all remaining chemicals were purchased from Sigma–Aldrich Co. (Budapest, Hungary). Fluorescent dye MitoTracker Red was obtained from Molecular Probes (Life Technologies, Carlsbad, CA, USA). Hematoxylin and eosin were purchased from Sigma–Aldrich Co. BGP-15 was a gift from N-Gene (New York, NY, USA). The following primer antibodies were used: anti-Akt, anti-phospho-Akt, anti-phospho-Akt substrate of 160 kDa (AS160), anti-phospho-mammalian target of rapamycin (mTOR), anti-phospho-p70 S6 kinase (S6K), anti-phospho-p44/42 MAPK (ERK1/2), anti-phospho-p38 MAPK (p38), anti-phospho-JNK MAPK (JNK1/2) (Cell Signaling Technology, Danvers, MA, USA), anti-glyceraldehyde-3-phosphate dehydrogenase (GAPDH) (EMD Millipore, Billerica, MA, USA), anti-Mfn1, anti-Mfn2, anti-Drp1, anti-Fis1 (Santa Cruz Biotechnology, Heidelberg, Germany) and anti-OPA1 (Invitrogen; Life Technologies, Carlsbad, CA, USA). The horseradish peroxidase-conjugated anti-mouse IgG and anti-rabbit IgG were obtained from Sigma–Aldrich Co., XF Calibrant, XF Base Medium and XFp Cell Mito Stress Test Kit including oligomycin, FCCP, rotenone/antimycin A were purchased from Agilent Technologies (Kromat Ltd., Budapest, Hungary). All reagents were of the highest purity commercially available.

2.2. Animals

Wistar male rats were purchased from Innovo Ltd. (Gödöllő, Hungary). The investigation conformed to the Guide for the Care and Use of Laboratory Animals published by the US National Institutes of Health, and was approved by the Animal Research Review Committee of the University of Pécs, Hungary. All animals were housed one or two per cage, under optimal laboratory conditions (controlled temperature, humidity and 12:12 h light-dark cycles) with free access to water and standard rodent chow. Starting at 8 weeks of age, the animals were assigned into four groups. Eight animals were allocated to control group receiving subcutaneous injection of isotonic saline (0.1 ml/kg) on day 0. Eight animals were allocated to BGP-15 group receiving subcutaneous injection of isotonic saline (0.1 ml/kg) on day 0 and BGP-15 (20 mg/kg per day, per os, in the drinking water) from day 0 to day 28. Eight animals were allocated to PAH group receiving 60 mg/kg subcutaneous injection of monocrotaline (MCT) on day 0. Eight animals were allocated to PAH + BGP-15 group receiving 60 mg/kg subcutaneous injection of MCT on day 0 and BGP-15 (20 mg/kg per day, per os, in the drinking water) from day 0 to day 28.

2.3. Cell cultures

WRL-68 (HeLa derivative), C2C12 (mouse C3H muscle myoblast), A549 (human lung carcinoma) and Sf9 (derived from pupal ovarian tissue of *Spodoptera frugiperda*) cell lines were obtained from the European Collection of Cell Cultures (Salisbury, UK). The WRL-68, C2C12 and A549 cell lines were maintained in a humidified 5% CO_2 atmosphere at 37 °C while Sf9 cells were cultured in a 100% air atmosphere at 27 °C. WRL-68 cells were cultured in Eagle's minimum essential medium (MEM), C2C12 and A549 cells in Dubelcco modified Eagle's medium (DMEM) (PAA Laboratories) while Sf9 cells in TC-100 insect medium (Sigma–Aldrich Co.). All media contained 10% bovine serum and antibiotic solution (1% penicillin and streptomycin mixture) (Gibco/Invitrogen). Cells were passaged at 3-day intervals.

Cells were seeded at a starting density of 5×10^5 cells/well in a 6-well plate for immunoblotting and at a density of 1×10^5 cells/well for fluorescent or confocal laser scanning microscopy.

2.4. Immunoblot analysis

The WRL-68 cells were seeded into a 6-well plate and cultured overnight. After subjecting the cells to 50 μM BGP-15 for 3 h, the cells were harvested in ice-cold lysis buffer containing 0.5 mM sodium metavanadate, 1 mM ethylenediaminetetraacetic acid (EDTA), and protease inhibitor mixture in phosphate-buffered saline (PBS). The proteins were precipitated by trichloroacetic acid, washed three times with −20 °C acetone, and subjected to sodium-dodecyl sulphate polyacrylamide gel electrophoresis. Proteins (20 μg/lane) were separated on 12% gels and then transferred to nitrocellulose membranes. The membranes were blocked in 5% low-fat milk for 1 h at room temperature and then exposed to primary antibodies at 4 °C overnight at the manufacturer's proposed dilution in blocking solution. Appropriate horseradish peroxidase-conjugated secondary antibodies were used for 2 h at room temperature in 1:5000 dilution. Peroxidase labeling was visualized with enhanced chemiluminescence using the SuperSignal West Pico chemiluminescent substrate (Life Technologies).

2.5. Construction of mitochondria-directed red and green fluorescent proteins

Mitochondria-directed enhanced red fluorescent protein (mERFP) expressing plasmid was constructed as follows: The mitochondrial targeting sequence (MTS) was amplified by polymerase chain reaction (PCR) from cytochrome *c* oxidase subunit VIIIa (COX8A) gene (RZPD), and the amplified sequence was inserted into pDsRed-Monomer-N1 mammalian expression plasmid (Clontech, Takara Bio Europe, Saint-Germain-en-Laye, France) between XhoI and HindIII restriction sites.

Construction of plasmid for the expression of mitochondria-directed enhanced green fluorescent protein (mEGFP) are described below: MTS was amplified from cytochrome *c* oxidase subunit VIIIa coding sequence (from RZPD) by PCR and ligated into pEGFP-N3 mammalian expression plasmid (Clontech) between BglII and SalI restriction sites.

2.6. Polyethylene glycol (PEG) fusion assay

The PEG fusion assay was performed as described previously [34]. Briefly, WRL-68 cells were transiently transfected with mERFP or mEGFP fluorescent protein. The next day, the PEG fusion assays were then performed. WRL-68 cells expressing mERFP were co-plated with WRL-68 cells expressing mEGFP on glass coverslips. Cycloheximide (20 μg/ml) was added 30 min before fusion. The 70–100% confluent cells in a 35-mm culture dish were then washed with MEM without serum and incubated for exactly 1 min with 750 μl of a prewarmed (37 °C) solution of PEG 1500 (50% [wt/vol] in MEM, Sigma–Aldrich Co.). The cultures were fixed in 4% formalin, and the cells were visualized by Nikon Eclipse Ti-U fluorescent microscope equipped with a Spot RT3 camera using a 60× objective and epifluorescent illumination.

2.7. Suppression of Akt, Mfn1, Mfn2 or OPA1 expression by siRNA

WRL-68 cells were transiently transfected with siRNA designed by the manufacturer (Santa Cruz Biotechnology) to silence Akt, Mfn1, Mfn2 or OPA1 in Opti-MEM I reduced serum medium using Lipofectamine 2000. Silencing efficiency was tested by immunoblot, using a polyclonal anti-Akt, anti-Mfn1, anti-Mfn2 or anti-OPA1 primary antibody.

2.8. Determination of mitochondrial fragmentation

WRL-68, C2C12 and A549 cells were seeded on glass coverslips and cultured at least overnight before the experiment. The cells were either transiently transfected with mERFP or treated and labeled using MitoTracker Red (50 nM) dye. Next day after transfection, cells were washed twice in PBS, and then treated as indicated in the text. After two washings, cells were fixed in 4% formalin and visualized by Olympus FluoView 1000 confocal laser scanning microscope. Excitation by multiline argon-ion laser at 488 nm and green helium-neon laser at 543 nm was used, respectively, for 10 μs/pixel in photon counting and sequential mode. The field of interest was scanned in XYZ mode, scanning the total thickness of the cells with 1.5 μm layer distance taking 1024 × 1024 pixel/layer images. 3D reconstruction of samples was achieved by the Imaris 4.2.0 software (Bitplane, Concord, MA, USA). Quantitative determination of mitochondrial fragmentation was performed as described before [35], and we considered as fragmented mitochondria those shorter than 2 μm and as filamental mitochondria those longer than 5 μm. MitoTracker Red labeled cells were visualized by Nikon Eclipse Ti-U fluorescent microscope equipped with a Spot RT3 camera using a 60× objective and epifluorescent illumination. The mitochondrial images were binarized by the 'threshold' module in ImageJ, and these binary images were converted to images 1 pixel wide by the 'skeletonize' module. Finally, mitochondrial length was determined using the 'analyze particles' module. Analyses were performed by an investigator blind to the experiment on at least 25 randomly chosen cells.

2.9. OPA1 GTPase assay and OPA1-OPA1 interactions

Mutant human OPA1 construct was made by GeneCust (Luxembourg, Germany). Chemically synthetized polynucleotide/DNA corresponding to human OPA1 (Genbank NM_015560.2) amino acid residues 210–960 and 8 His was inserted into pFastBac 1 plasmid vector (Invitrogen Life Technologies) between SalI and NotI restriction sites. His-tagged OPA 1 mutant protein was expressed in Sf9 cells and purified from cell pellets using Ni-NTA agarose beads (Sigma–Aldrich Co.) according to the corresponding manual. OPA1 GTPase reactions were performed with 0–0.150 μg/ml OPA1 in 50 mM hydroxyethyl piperazine ethanesulfonic acid (HEPES; pH 7.0), 1 mM dithiothreitol at 300 mM NaCl concentrations, and the GTP hydrolysis was quantified by monitoring the released free phosphate using a malachite green assay at 37 °C for 90 min.

Amino functionalized magnetic micro particles from Sigma–Aldrich Co. were activated by glutaraldehyde as described in the manual. Recombinant OPA1 was immobilized to magnetic beads; 2 μg OPA1 to 60 μg magnetic particles. The reaction took place for 180 min and was blocked with 100 mM ethanolamide for 60 min. Magnetic beads were washed three times with reaction buffer; 5 mM HEPES containing 150 mM NaCl, 2 mM $MgCl_2$ at pH 8.0. OPA1-OPA1 interactions were determined in 0.5 ml reaction buffer containing 60 μg OPA1 immobilized magnetic particles and 6 μg recombinant OPA1, shaken for 60 min at 25 °C, separated and non-covalently bound OPA1 was removed from the beads by 1 M ammonium hydroxide and its quantity was determined by enzyme-linked immunosorbent assay (ELISA).

2.10. Determination of oxygen consumption

Oxygen consumption rate (OCR) was determined by Agilent Seahorse XFp Analyzer (Kromat Ltd.). A549 cells were seeded in XFp Miniplate at the density of 1.5×10^4 cells/well in 80 μl complete growth medium (DMEM containing 10% FBS) and incubated at 37 °C, 5% CO_2 for 24 h. On the day prior to assay, XFp Sensor Cartridge was hydrated in XF Calibrant at 37 °C in a non-CO_2 incubator overnight. On the day of the assay, cells were treated for 3 h with 0 (control) or 10 μmol/10^7 cells H_2O_2 in the absence or presence of BGP-15 (50 μM). After the treatment, complete growth medium was removed and replaced with assay medium consisting of Agilent XF Base Medium supplemented with 10 mM glucose, 1 mM pyruvate and 2 mM glutamine, pH 7.4. The plate was placed into a 37 °C non-CO_2 incubator for 1 h. Before the measurement, oligomycin, carbonyl cyanide 4-(trifluoromethoxy)phenylhydrazone (FCCP) and rotenon/antimycin A were loaded in the injection ports of the sensor cartridge. Final concentration of the aforementioned compounds was 1 μM and three measurements were taken after each injection.

2.11. Lung histology

Lungs were removed on day 28 after euthanasia by isoflurane inhalation, quickly blotted free of blood, weighed, and processed as required for histology. Lungs from 4 rats of each group were fixed in 6% formalin, embedded in paraffin, and sectioned 5 μm thin by a microtome. The sections were stained with hematoxylin–eosin, and digital photos were taken. Average wall thickness of alveolar sac was determined at randomly chosen 25 different sites in each section. Macrophages were counted in 10 non-overlapping high power fields (200×) in each section by an expert who was blind to the experiment.

2.12. Electron microscopy

For electron microscopy analysis, 1–2 mm^3 blocks were cut from lung samples and fixed using modified Kranovsky fixative (2% paraformaldehyde, 2.5% glutaraldehyde, 0.1 M Na-cacodylate buffer, pH 7.4 and 3 mM $CaCl_2$). After samples were washed in phosphate buffer, they were incubated in 1% osmium tetroxide in 0.1 M PBS for 35 min. Samples were then washed in buffer several times for 10 min and dehydrated in an ascending ethanol series, including a step of uranyl acetate (1%) solution in 70% ethanol to increase contrast. Dehydrated blocks were transferred to propylene oxide before being placed in Durcupan resin (Sigma–Aldrich Co.) and then embedded in gelatin capsules containing Durcupan. The blocks were placed in an incubator for 48 h at 56 °C. From the embedded blocks, 1 μm thick semithin and serial ultrathin sections (70 nm) were prepared with a Leica ultramicrotome and mounted on mesh or on collodion-coated (Parlodion, Electron Microscopy Sciences, Fort Washington, PA, USA), single-slot, copper grids. Additional contrast was provided with uranyl acetate and lead citrate solutions; sections were then examined using a JEOL1200EX-II electron microscope.

2.13. Statistics

All data were expressed as means ± standard error of mean (SEM) from replicate determinations. ANOVA with a post hoc correction was used to determine differences. The Student's *t* test was used to compare the mean values of two groups. Differences were regarded as significant when the p value was $< .05$.

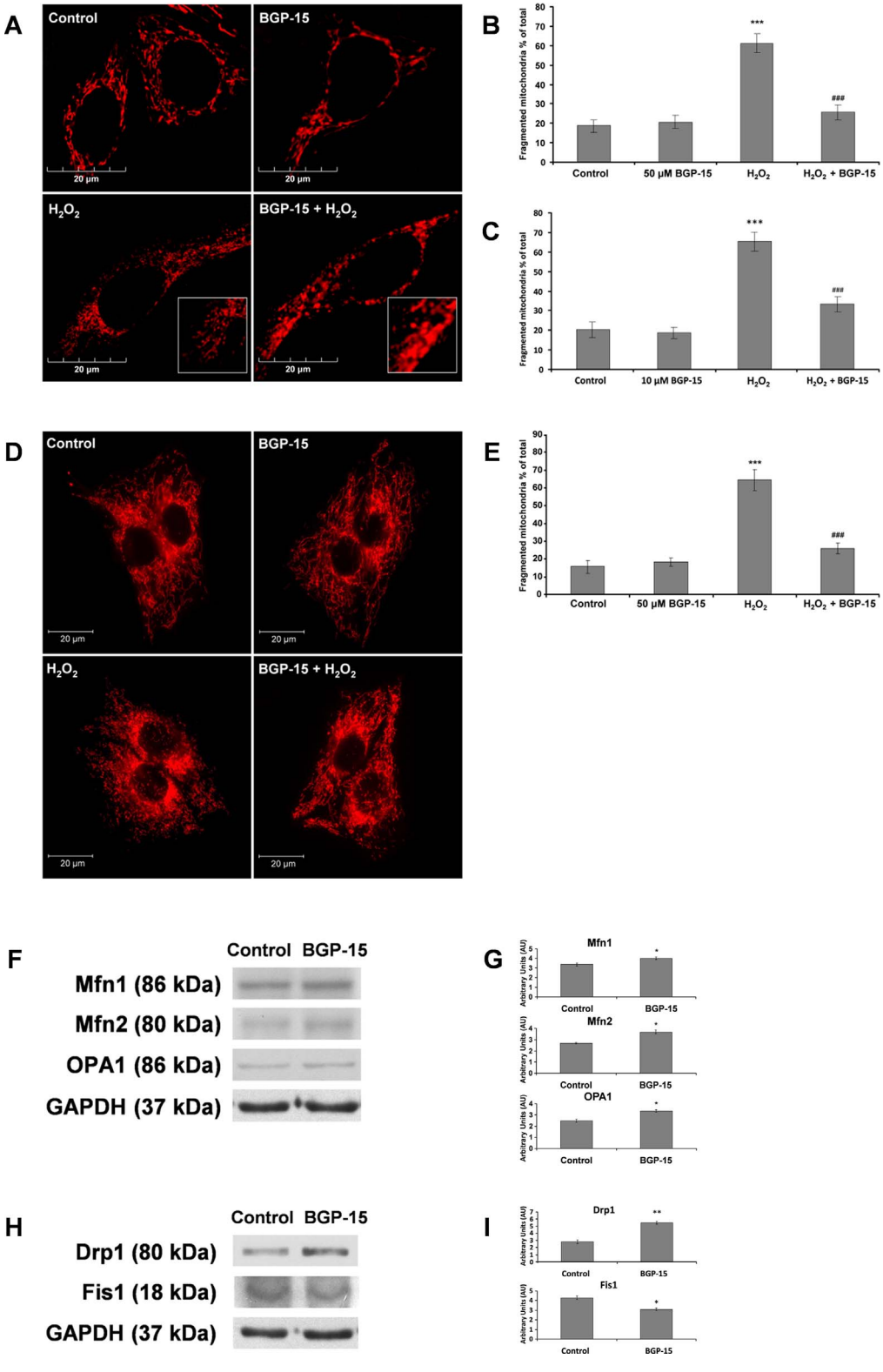

Fig. 1. BGP-15 protects against oxidative stress-induced mitochondrial fragmentation in WRL-68 cells and C2C12 muscle myoblasts. (A) BGP-15 (50 µM) protects against oxidative stress-induced (10 µmol/10^7 cells H_2O_2) mitochondrial fragmentation in WRL-68 cells; fragmented mitochondria were shorter than 2 µm and filamental mitochondria were longer than 5 µm. Mitochondria were labeled by mitochondria directed-ERFP. (B) Quantitative analysis of H_2O_2-induced mitochondrial fragmentation and its reduction by BGP-15 (50 µM) in WRL-68 cells. (C) Quantitative analysis of H_2O_2-induced mitochondrial fragmentation and its reduction by BGP-15 (10 µM) in WRL-68 cells. (D) BGP-15 (50 µM) protects against oxidative stress-induced (50 µM H_2O_2) mitochondrial fragmentation in C2C12 muscle myoblast cells. Mitochondria were visualized by 50 nM MitoTracker Red. (E) Quantitative analysis of the protective effect of BGP-15 against oxidative stress-induced mitochondrial fragmentation in C2C12 muscle myoblast cells. (F) BGP-15 (50 µM) increases the expression of mitochondrial fusion proteins - Mfn1, Mfn2 and OPA1- determined by immunoblot in WRL-68 cells. (G) Quantitative analysis of effect of BGP-15 on Mfn1, Mfn2 and OPA1. (H) BGP-15 (50 µM) increases the expression of mitochondrial fission protein Drp1 and decreases the expression of Fis1 determined by immunoblot in WRL-68 cells. (I) Quantitative analysis of effect of BGP-15 on Drp1 and Fis1. Data are presented as mean ± SEM of three independent experiments. In (B, C and E) *** $p \leq .001$ compared to control cells; ### $p \leq .001$ compared to H_2O_2 treated cells. In (G and I) * $p \leq .05$ ** $p \leq .01$ compared to control group (Student's *t*-test)

3. Results

3.1. BGP-15 attenuated oxidative stress-induced mitochondrial fragmentation

Based on our previous studies [24–33], we assumed that BGP-15 affects mitochondrial fusion/fission. Dose-dependently [36], H_2O_2 induces various cellular damages; at the dose of 10 µmol/10^7 cells it caused mitochondrial fission resulting in fragmented mitochondria within 4–6 h that was detected by either MitoTracker Red staining, or by mERFP transfection (Fig. 1). H_2O_2-induced mitochondrial fragmentation was significantly reduced by 10–50 µM BGP-15 in mERFP-labeled WRL-68 cells (Fig. 1A–C). In C2C12 mouse muscle myoblasts, treatment with 10 µmol/10^7 cells H_2O_2 for 5 h induced mitochondrial fragmentation, which was also prevented by treatment with BGP-15 (Fig. 1D and E).

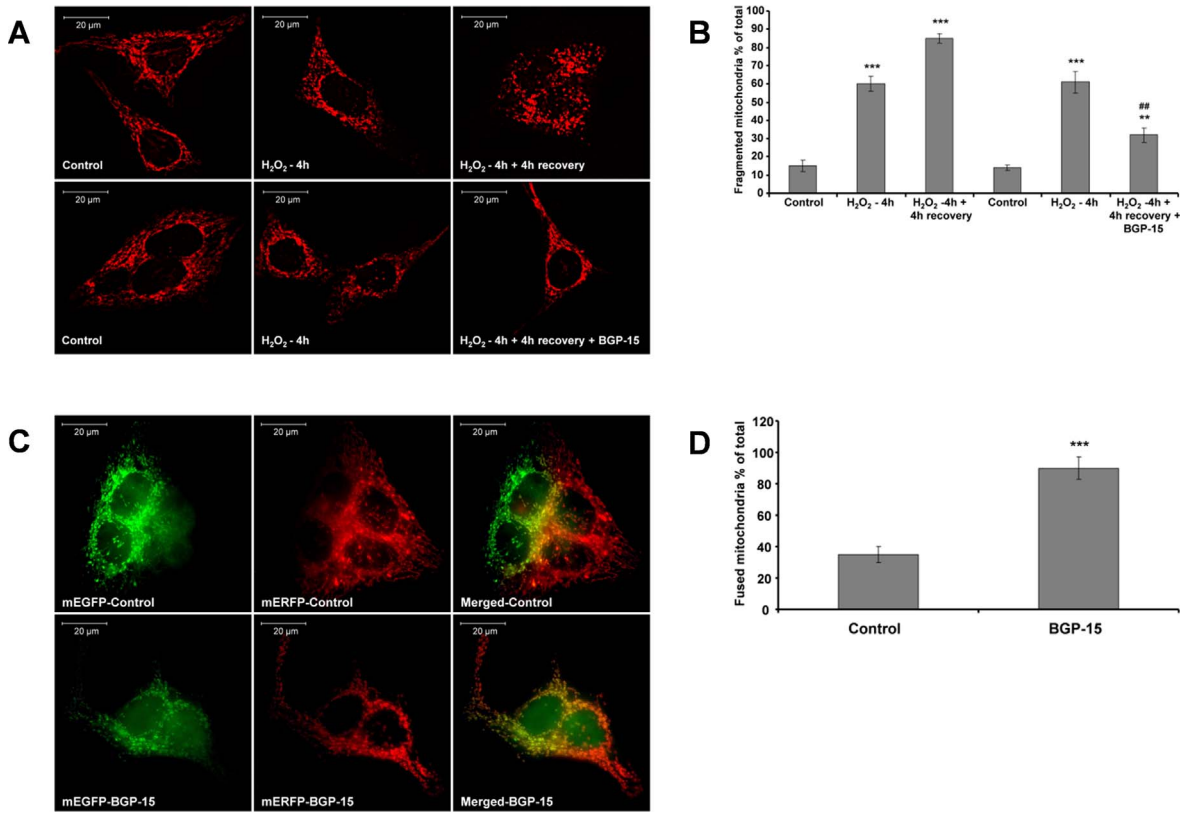

Fig. 2. BGP-15 activates mitochondrial fusion in WRL-68 cells. (A) Mitochondrial fragmentation was induced by H_2O_2 (10 μmol/10^7 cells) for 4 h, and fragmented mitochondria were kept in fresh original media, or in fresh media containing 50 μM BGP-15 for another 4 h. Mitochondria were visualized by 50 nM MitoTracker Red. (B) Quantitative analysis of BGP-15 activated mitochondrial fusion of fragmented mitochondria. (C) BGP-15 facilitates mitochondrial fusion after PEG-mediated cell fusion of mEGFP and mERFP labeled WRL-68 cells. (D) Quantitative analysis of BGP-15 activated mitochondrial fusion after PEG-mediated cell fusion. Data are presented as mean ± SEM of three independent experiments. ** $p \leq .01$ and *** $p \leq .001$ compared to control cells; $^{\#\#}$ $p \leq .01$ compared to H_2O_2 treated cells (Student's *t*-test).

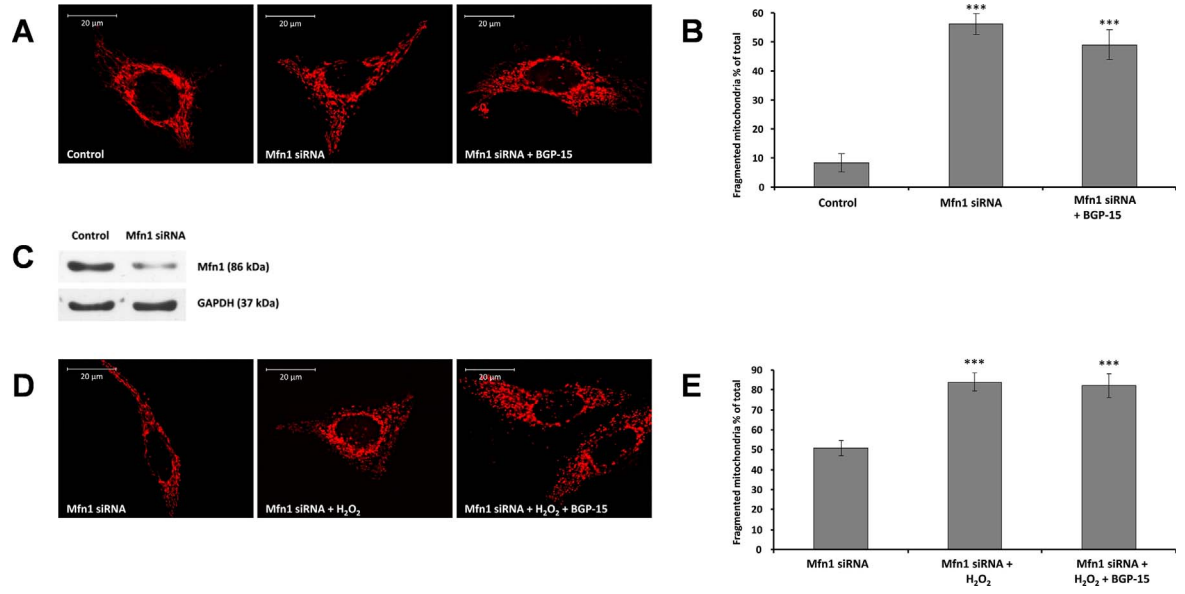

Fig. 3. Suppression of Mfn1 -a critical component of outer mitochondrial fusion machinery- prevents BGP-15 induced mitochondrial fusion in WRL-68 cells. (A) Suppression of Mfn1 induces mitochondrial fragmentation and attenuates BGP-15-promoted mitochondrial fusion. Mitochondria were visualized by 50 nM MitoTracker Red. (B) Quantitative analysis of mitochondrial fragmentation induced by Mfn1 suppression. (C) Immunoblot showing the suppression of Mfn1 by siRNA. (D) Mfn1 suppression abolishes BGP-15-induced (50 μM) mitochondrial fusion in oxidative stress (10 μmol/10^7 cells H_2O_2, 5 h). (E) Quantitative analysis of BGP-15-induced mitochondrial fusion in Mfn1-suppresed cells in oxidative stress. Data are presented as mean ± SEM of three independent experiments. In (B), *** $p \leq .001$ compared to control cells; in (E), *** $p \leq .001$ compared to Mfn1-suppressed cells (Student's *t*-test).

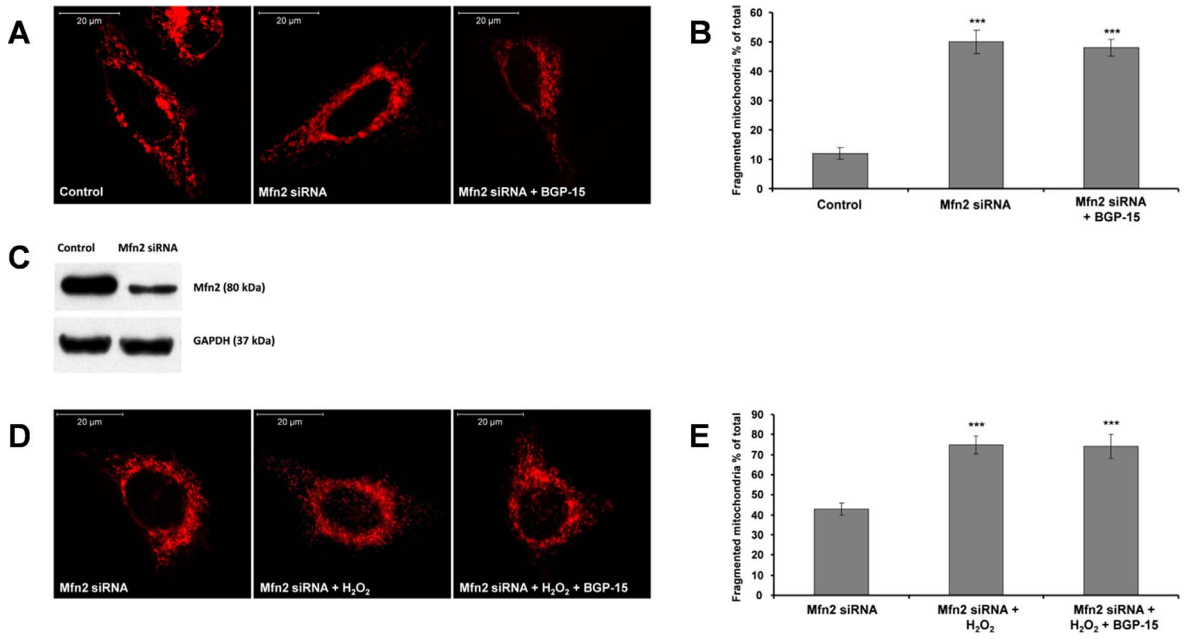

Fig. 4. Suppression of Mfn2-a critical component of outer mitochondrial fusion machinery- prevents BGP-15 induced mitochondrial fusion in WRL-68 cells. (A) Suppression of Mfn2 induces mitochondrial fragmentation and attenuates BGP-15-promoted mitochondrial fusion. Mitochondria were visualized by 50 nM MitoTracker Red. (B) Quantitative analysis of mitochondrial fragmentation induced by Mfn2 suppression. (C) Immunoblot showing the suppression of Mfn2 by siRNA. (D) Mfn2 suppression abolishes BGP-15-induced (50 µM) mitochondrial fusion in oxidative stress (10 µmol/10^7 cells H_2O_2, 5 h). (E) Quantitative analysis of BGP-15-induced mitochondrial fusion in Mfn2-suppresed cells in oxidative stress. Data are presented as mean ± SEM of three independent experiments. In (B), *** $p \leq .001$ compared to control cells; in (E), *** $p \leq .001$ compared to Mfn2-suppressed cells (Student's *t*-test).

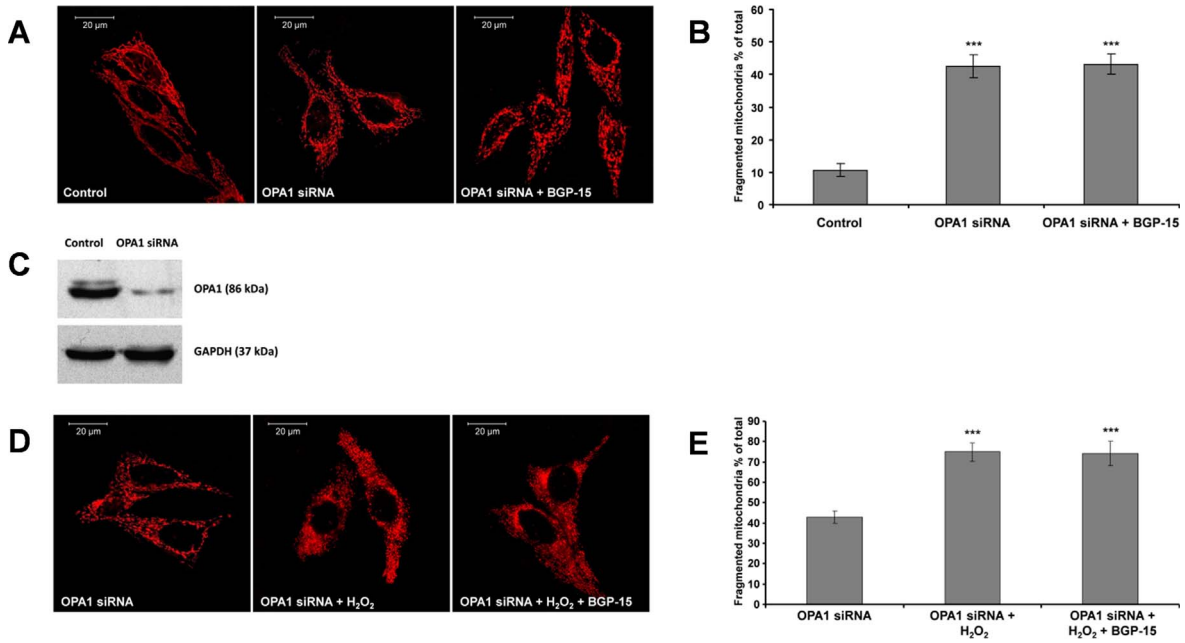

Fig. 5. Suppression of OPA1 -a critical component of inner mitochondrial fusion machinery- prevents BGP-15 induced mitochondrial fusion in WRL-68 cells. (A) Suppression of OPA1 induces mitochondrial fragmentation and prevents BGP-15 promoted mitochondrial fusion. Mitochondria were visualized by 50 nM MitoTracker Red. (B) Quantitative analysis of mitochondrial fragmentation in OPA1-suppresed cells. (C) Immunoblot showing the suppression of OPA1 by siRNA. (D) BGP-15 (50 µM) cannot prevent oxidative stress-induced (10 µmol/10^7 cells H_2O_2, 5 h) mitochondrial fragmentation in OPA1-suppresed cells. (E) Quantitative analysis of BGP-15-induced mitochondrial fusion in OPA1-suppresed cells in oxidative stress. Data are presented as mean ± SEM of three independent experiments. In (B), *** $p \leq .001$ compared to control cells; in (E), *** $p \leq .001$ compared to OPA1-suppressed cells (Student's *t*-test).

In addition, we analyzed the effect of BGP-15 on the expression of mitochondrial fusion related genes. These data show that BGP-15 treatment causes small but significant increases in the expression of mitochondrial fusion proteins Mfn1, Mfn2 and OPA1 determined by immunoblot analysis (Fig. 1F and G). Analysis of mitochondrial fission proteins Drp1 and Fis1 give contradictory data, namely increased Drp1 expression but decreased Fis1 expression after BGP-15 treatment (Fig. 1H and I). Therefore, it was difficult to draw any conclusion from these results, although it seemed more likely that BGP-15 increased mitochondrial fusion rather than reducing fission.

3.2. BGP-15 promoted fusion

Next, we treated WRL-68 cells with 10 µmol/10^7 cells H_2O_2 for 4 h,

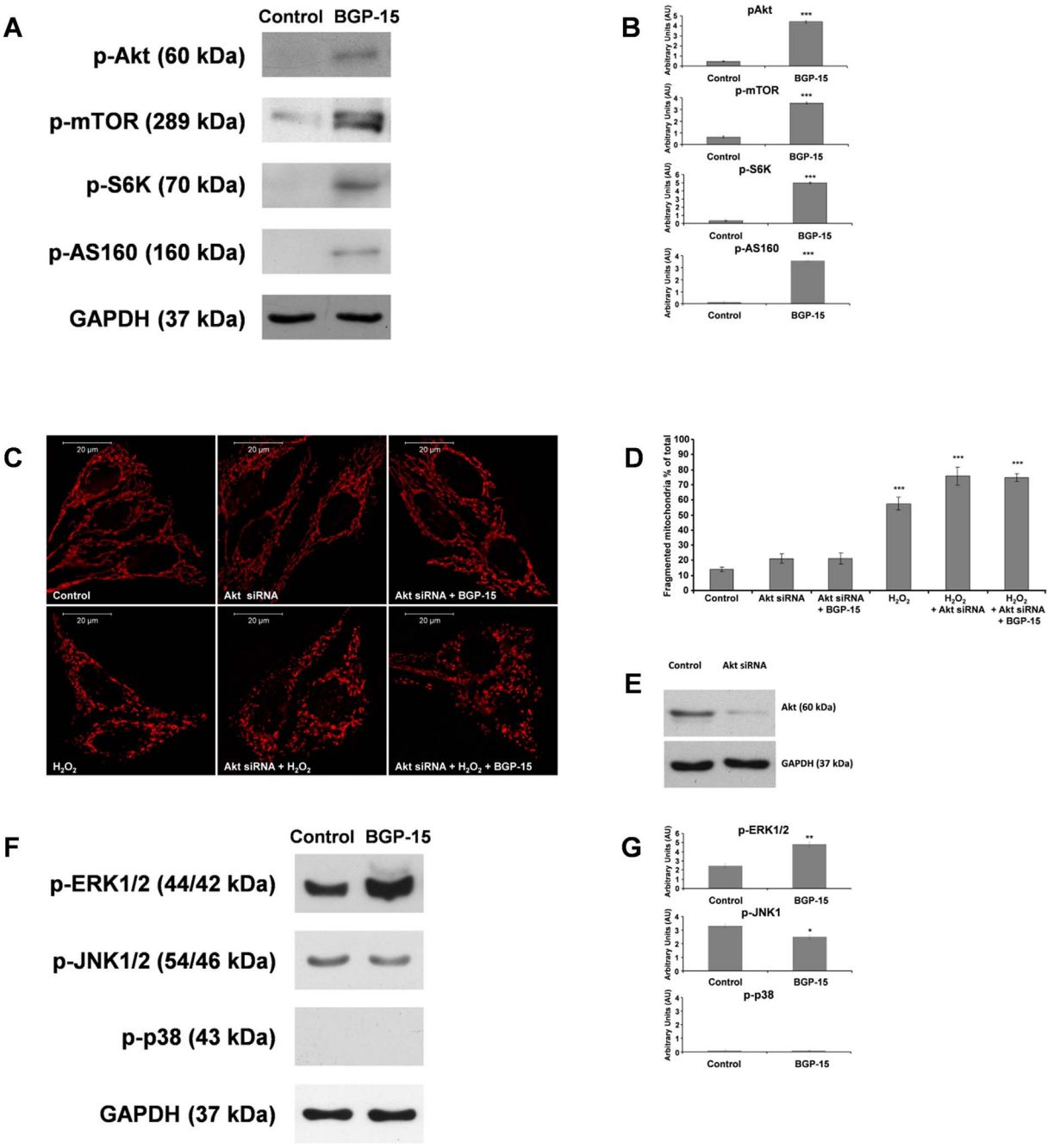

Fig. 6. Critical role of Akt in BGP-15-activated mitochondrial fusion in WRL-68 cells. (A) Effect of BGP-15 (50 μM) on Akt-AS160 and Akt-mTOR pathways. (B) Quantitative analysis of effect of BGP-15 on Akt-AS160 and Akt-mTOR pathways. (C) Effect of BGP-15 on mitochondrial fragmentation, and oxidative stress-induced (10 μmol/10^7 cells H_2O_2, 5 h) fragmentation in Akt suppressed cells. Mitochondria were visualized by 50 nM MitoTracker Red. (D) Quantitative analysis of effect of BGP-15 on mitochondrial fragmentation in Akt suppressed cells. (E) Immunoblot showing the suppression of Akt by siRNA. (F) Effect of BGP-15 (50 μM) on MAPK phosphorylation (JNK, ERK and p38). (G) Quantitative analysis of effect of BGP-15 on JNK, ERK and p38 MAPK. We failed to detect JNK2 phosphorylation under our experimental conditions. Data are presented as mean ± SEM of three independent experiments. In (B and G), * $p \leq .05$, ** $p \leq .01$ and *** $p \leq .001$ compared to control group; in (D), *** $p \leq .001$ compared to control cells (Student's *t*-test).

and, as expected, mitochondrial fragmentation was detected by MitoTracker Red labeling (Fig. 2A and B). After the H_2O_2 treatment, the medium was replaced to a fresh one containing or not 50 μM BGP-15 to determine the reformation of mitochondrial filaments. Cells cultured in control medium for 4 h were unable to reform mitochondrial filaments (Fig. 2A and B) while cells cultured in medium containing 50 μM BGP-15 for 4 h were able to recover and reform mitochondrial filaments likely by activation of fusion.

3.3. Measuring mitochondrial fusion by mitochondrial matrix targeted green and red fluorescent proteins

To confirm this observation with an independent method, WRL-68 cells were transfected with mERFP, or mEGFP, were mixed, and fused using PEG. After the removal of PEG, the cells were cultured and treated with 50 μM BGP-15 for 5 h and fixed. Mitochondrial fusion was detected by fluorescent microscopy (Fig. 2C). The rate of migration of red and green fluorescence proteins to the other cells showed that mitochondrial fusion occurred in control cells (Fig. 2C and D), but BGP-15 displayed a much faster rate of mitochondrial fusion, as determined by

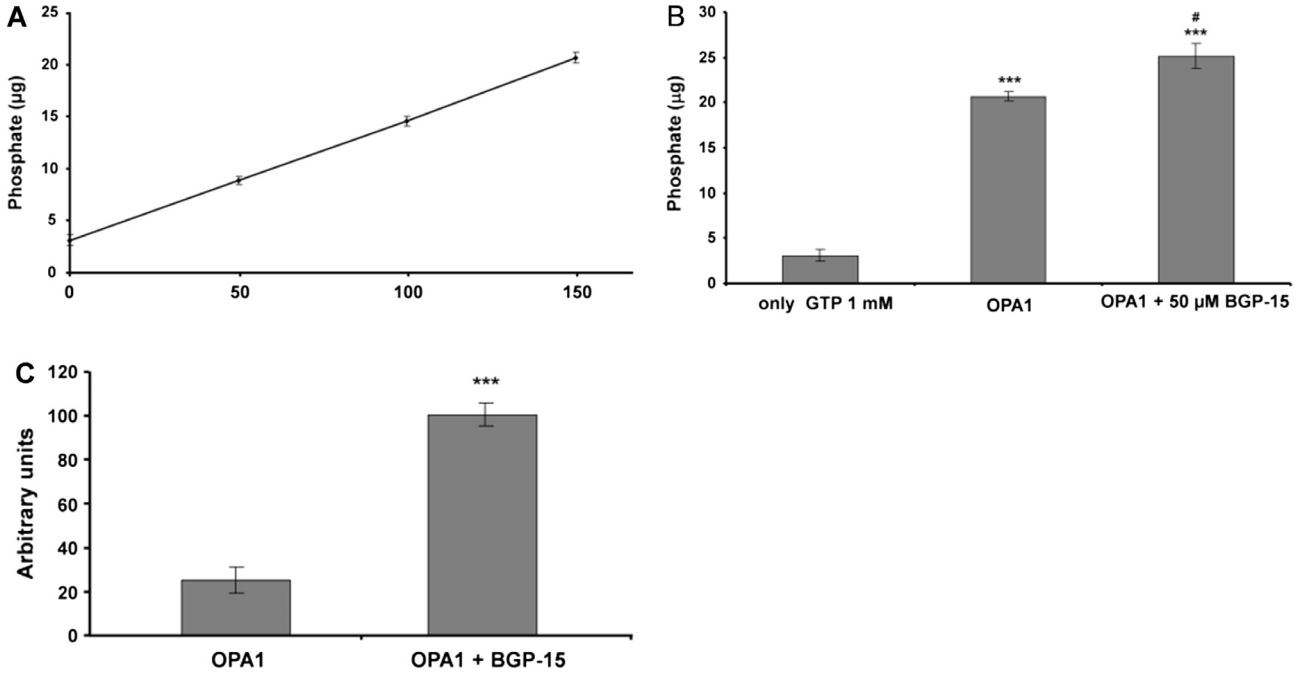

Fig. 7. BGP-15 facilitates GTPase activity and self-aggregation of OPA1. (A) GTP-ase activity of recombinant OPA1 (amounts in µg/ml are depicted on x axis) was assessed by measuring the released inorganic phosphate (y axis) by malachite green assay. (B) Effect of BGP-15 on the GTPase activity of recombinant OPA1. Released phosphate (y axis) resulting from spontaneous hydrolysis of GTP (only GTP 1 mM), hydrolysis assisted by 150 µg/ml recombinant OPA1 (OPA1) and 150 µg/ml recombinant OPA1 + 50 µM BGP-15 (OPA1 + BGP-15). (C) BGP-15 promotes OPA1-OPA1 interactions. Aggregate formation (y axis) in the absence (OPA1) and presence (OPA1 + BGP-15) of BGP-15. Data are presented as mean ± SEM of three independent experiments. In (B), *** $p \leq .001$ compared to enzyme free group, # $p \leq .05$ compared to OPA1 group; in (C), *** $p \leq .001$ compared to OPA1 group (Student's *t*-test).

the faster migration rate of red or green fluorescent protein into the mitochondria of the neighboring cells (Fig. 2C and D). These experiments show that BGP-15 promoted mitochondrial fusion in living cells.

3.4. BGP-15-induced mitochondrial fusion required active outer membrane and inner membrane fusion machinery

Mfn1 and Mfn2-essential proteins of mitochondrial outer membrane fusion-were suppressed by siRNA that induced some level of mitochondrial fragmentation in unstressed cells (Figs. 3A and B and 4A and B), which could not been reversed by BGP-15 (Figs. 3A and B and 4A and B). Oxidative stress induced further mitochondrial fragmentation in Mfn1 and Mfn2 silenced cells, and again, BGP-15 could not rescue mitochondria from ROS-induced fragmentation (Figs. 3D and E and 4D and E) indicating that outer membrane fusion machinery is required for the protective effect of BGP-15 (Figs. 3A, B, D and E and 4A, B, D and E).

OPA1 plays an essential role in fusion of the inner mitochondrial membrane; its suppression by siRNA induced more mitochondrial fragmentation as compared to normal cells (Fig. 5A and B). BGP-15 (50 µM) could not reverse this partial fragmentation (Fig. 5A and B). Oxidative stress further increased mitochondrial fragmentation, and BGP-15 was again ineffective to prevent it (Fig. 5D and E).

3.5. Akt activation was required for mitochondrial fusion

BGP-15 activated Akt and induced the phosphorylation of some related kinases, mTOR, S6K and AS160 (Fig. 6A and B); a process that can play important role in the protection of mitochondrial membrane systems [37,38]. Therefore, we analyzed the effect of Akt suppression on BGP-15 induced fusion. Fig. 6C and D show that silencing of Akt induced mitochondrial fragmentation. Oxidative stress-induced mitochondrial fragmentation was significantly reduced by BGP-15 in normal cells (Fig. 1A–C); however, BGP-15 could not prevent or reduce ROS-induced mitochondrial fragmentation in Akt suppressed cells (Fig. 6C and D). These data show that active Akt is required for mitochondrial fusion, and the BGP-15-mediated prevention of mitochondrial fragmentation requires Akt. We studied the effect of BGP-15 on the MAPKs; BGP-15 significantly activated ERK1/2 phosphorylation and reduced JNK1 phosphorylation (Fig. 6F and G), which could be advantageous for mitochondrial function. Phosphorylation of p38 was too low to detect under our experimental conditions (Fig. 6F and G).

3.6. BGP-15 facilitated GTPase activity and self-aggregation of OPA1

The protective effect of BGP-15 in cristae membrane damages suggests a role of OPA1 in BGP-15-mediated mitochondrial protection. OPA1 GTPase assay showed that recombinant short OPA1 hydrolyzed GTP in a concentration dependent manner (Fig. 7A), as expected. BGP-15 facilitated GTP hydrolysis by OPA1 (Fig. 7B), which process may have contributed to the bioenergetics basis of mitochondrial cristae protection. This observation suggests also that OPA1 can be the first direct molecular target of BGP-15. Since BGP-15 activates GTP hydrolysis by OPA1 (Fig. 7B), it can provide more energy to hold together mitochondrial cristae membranes and activates mitochondrial fusion.

Also, we analyzed the effect of BGP-15 on the OPA1-OPA1 interaction (Fig. 7C), by crosslinking OPA1 protein to amino groups containing magnetic beads and studying the interaction between immobilized OPA1 and free OPA1 in the solution. Fig. 7C shows that BGP-15 increased aggregation of OPA1 on the magnetic beads, providing direct evidence that BGP-15 increased the interactions between OPA1 molecules.

3.7. Evidence for the BGP-15-induced mitochondrial fusion in vivo in pulmonary arterial hypertension model

A549 lung epithelial cells demonstrated many long mitochondrial filaments under normal conditions, while oxidative stress induced mitochondrial fragmentation and the disappearance of the mitochondrial filaments (Fig. 8A and B). Adding BGP-15 to the media prevented the intensive mitochondrial fragmentation induced by oxidative stress, and

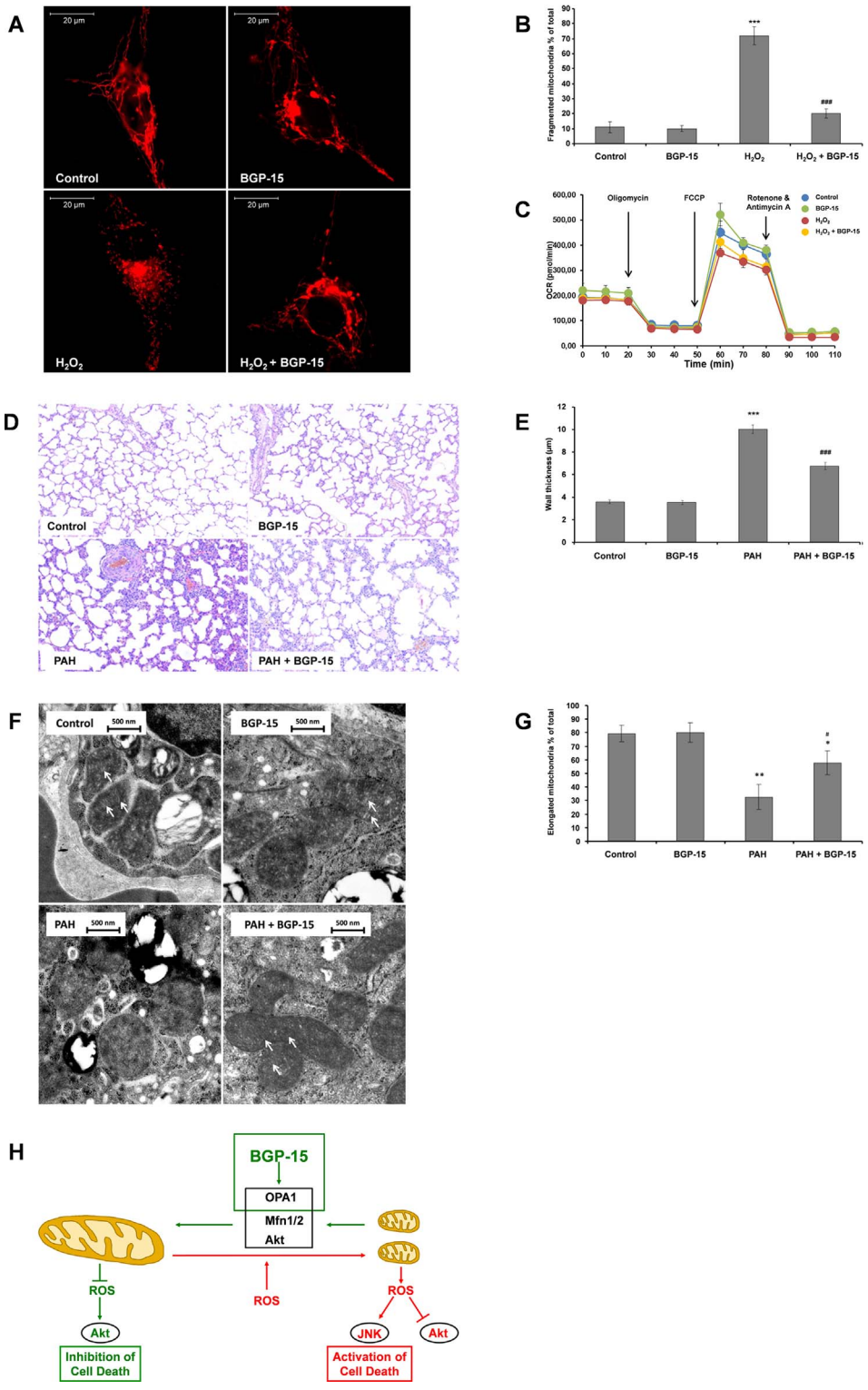

Fig. 8. BGP-15 activates mitochondrial fusion *in vivo* in PAH. (A) BGP-15 (50 μM) protects against oxidative stress-induced (10 μmol/10^7 cells H_2O_2, 5 h) mitochondrial fragmentation in A549 lung epithelial cells. Mitochondria were visualized by 50 nM MitoTracker Red. (B) Quantitative analysis of the protective effect of BGP-15 against oxidative stress-induced mitochondrial fragmentation. (C) Effect of BGP-15 and H_2O_2 on the oxygen consumption rate (OCR) in A549 cells measured by Seahorse FXp Analyzer. (D) Effect of BGP-15 on MTC-induced lung damages in PAH model. Formalin fixed lungs sections were stained by hematoxylin eosin, and subjected to histopathological analysis. Representative stained sections are presented. (E) Quantitative analysis of mean wall thickness of alveolar sac in PAH model (n = 4 rats for each group). (F) Effect of BGP-15 on mitochondrial structure of lung type II pneumocytes in MCT-induced PAH model by electron microscopy. (G) Quantitative analysis of effect of BGP-15 on mitochondrial structure in MCT-induced PAH model. (H) Schematic model for BGP-15 induced mitochondrial fusion and Akt activation leading to prevention of cell death. Red and green colors denote the action of ROS and BGP-15, respectively. Pointed arrows represent activation while flat ones inhibition. Data are presented as mean ± SEM of three independent experiments. In (B), *** $p \leq .001$ compared to control cells, $^{###}$ $p \leq .001$ compared to H_2O_2 treated cells; in (E), *** $p \leq .001$ compared to control group, $^{###}$ $p \leq .001$ compared to PAH group; in (G) * $p \leq .05$, ** $p \leq .01$ compared to control group, $^{\#}$ $p \leq .05$ compared to PAH group (Student's *t*-test).

kept mitochondria predominantly in the filamentous state (Fig. 8A and B). The effect of BGP-15 (50 μM) and H_2O_2 (10 μmol/10^7) on the OCR was determined by Seahorse XFp Analyzer (Fig. 8C). BGP-15 did not modify the rate of mitochondrial respiration. H_2O_2 induced a slight decrease, while BGP-15 induced a small, but not significant increase in OCR together with H_2O_2 compared to only H_2O_2. All of these data show that under our experimental conditions H_2O_2-induced inactivation of respiratory complexes does not play significant role in the BGP-15-mediated mitochondrial fusion processes.

In MCT-induced PAH, ROS initiates lung epithelial cell damage which contributes to disease development. Therefore, we analyzed the role of mitochondrial fragmentation in MCT-induced rat PAH model. Histopathological study of lung tissue in control and BGP-15 treated groups showed the alveolar sac and bronchioles with normal epithelium (Fig. 8D and E), while in MCT treated group small pulmonary vessels with inflammatory lesions and extensive vascular remodeling with intimal and medial hypertrophy of the muscular arteries as well as interstitial fibrosis could be detected. In addition, mean thickness of

alveolar sacs was highly increased (Fig. 8D and E). BGP-15 treated PAH animal lungs showed improved histological appearance, diminished infiltration with inflammatory cells, decreases in the thickness of alveolar sacs (Fig. 8D and E) indicating that BGP-15 imposed a major protective effect in PAH.

Transmission electron microscopic analysis showed severe damages in alveolar structure in lung of PAH rats compared to control and BGP-15 treated animals. The mitochondria of type II pneumocytes in control rats differed from the mitochondria of PAH rats. The structure of the mitochondrial cristae was normal, dense matrix was seen and the shape of mitochondria showed normal heterogeneity (ellipsoid, oval-shaped, rounded rod-like) in the control group as shown by arrows (Fig. 8F and G). Mitochondria of type II pneumocytes in PAH rats were often rounded and swollen, the mitochondrial matrix was very light and cristae structure was unclear. The mitochondrial ultrastructure in the PAH + BGP-15 group was similar to that of the healthy rats. The structure of the mitochondrial cristae was almost normal, dense matrix was seen and the mitochondria were less swollen (Fig. 8F and G). These data demonstrate that BGP-15 could prevent mitochondrial cristae membrane damages, and reduced mitochondrial fragmentation in an *in vivo* PAH model.

4. Discussion

It is well documented that ROS initiate mitochondrial fragmentation and contribute to the development and progression of various diseases [2,7,8]. Therefore, it would be very useful to find a way to reverse mitochondrial fragmentation. Here, we provide evidence that BGP-15 prevented oxidative stress-induced mitochondrial fragmentation in several cell lines and in an *in vivo* PAH model. These data suggest that BGP-15 might protect against ROS-induced damage *in vivo*, and to the best of our knowledge, it is the first small synthetic molecule that promotes mitochondrial fusion (Fig. 2).

We demonstrated that the prevention of ROS-induced mitochondrial fragmentation by BGP-15 required the existence of active outer and inner membrane fusion machinery; suppression of Mfn1, Mfn2 or OPA1 eliminated the effect of the drug (Figs. 3–5). These observations are supported by our previous data in different model systems showing that BGP-15 suppressed ROS production/oxidative damage, AIF release and caspase activation, and protected the respiratory chain from damage [26–28,39]. Furthermore, active mitochondrial fusion is important not only to maintain mitochondrial integrity and to reduce mitochondrial ROS production, but also to activate mitochondrial DNA (mtDNA) replication elevating mtDNA copy number [40].

Since BGP-15 reduce mitochondrial ROS production [39], we assumed that this effect can be related to OPA1 and its GTPase activity, because it was shown that the short isoform of OPA1 is responsible for maintaining of mitochondrial cristae structure and the oxidative phosphorylation function [41]. Here, we verified that BGP-15 activated GTP hydrolysis of recombinant OPA1 (Fig. 7). Therefore, BGP-15 acted in a unique fashion to trigger GTP hydrolysis of OPA1 that may represent the molecular mechanism underlying the fusion of inner mitochondrial membranes. Consequently, it is very likely that activation of mitochondrial fusion by synthetic small molecules affecting OPA1 function can be an effective way for the prevention of mitochondrial fragmentation.

Another way to prevent mitochondrial fragmentation is to inhibit or suppress Drp1, an essential mitochondrial fission protein. Inhibition of fission has positive effect on the short run [42,43], but on the long run it may cause problems with autophagy, development, and cell cycle regulation according to knockout mice data [44]. In addition, a recent publication suggests that the major cytoprotective effect of mitochondrial division inhibitor (mdivi-1) – a widely used Drp-1 inhibitor – is not induced via direct inhibition of Drp-1 but via the reversible inhibition of complex I resulting in reduced ROS production [45]. However, we found that BGP-15 does not modify mitochondrial oxidation at physiologically relevant concentrations (Fig. 8), suggesting that BGP-15 has a different molecular mechanism.

It is well established that significantly increased oxidative stress and mitochondrial fragmentation caused by the mutations in the dystrophin gene play role in the development of severe muscular dystrophy [16]. Therefore, the prevention of mitochondrial fragmentation by the activation of fusion could be advantageous in this disease. Previously, it was found that BGP-15 slowed the progression of severe muscular dystrophy in an animal model, and this effect was considered to be mediated via increasing heat shock protein (HSP) 72 expression [24]. However, it is more likely that BGP-15-induced activation of mitochondrial fusion and Akt can play a significant role in the reduced progression of muscular dystrophy. Moreover, BGP-15-induced Akt activation via inactivation of glycogen synthase kinase 3β (GSK-3β) can facilitate heat shock response preventing GSK-3β-induced inactivation of heat shock factor 1 [46] that may explain the role of HSP 72.

Whereas, oxidative stress and mitochondrial fragmentation also play significant role in the development of PAH [20,21], we investigated the potential mitochondrial fusion-inducing effect of BGP-15 on this *in vivo* model. We found that BGP-15 effectively maintained the structure of mitochondrial cristae and reduced MCT-induced mitochondrial fragmentation (Fig. 8).

In conclusion, the activation of mitochondrial fusion and the related Akt induction (Fig. 8H) can be protective mechanisms in a wide variety of diseases in which mitochondrial fission is important such as diabetes, muscular dystrophies, neurodegenerative diseases, and PAH. The induction of mitochondrial fusion by OPA1 GTPase activation may improve the survival and quality of life of patients with a number of common disorders.

Conflict of interest

Professor Mark A Febbraio is the Chief Scientific Officer and shareholder of N-Gene. Dr. Kengyel reports grants from ÚNKP-16-3 New National Excellence Program of the Ministry of Human Capacities during the conduct of the study. All remaining authors have declared that no competing interests exist.

Acknowledgments

This work was supported by Hungarian grants OTKA K-104220, OTKA NN-109841, GINOP-2.3.3-15-2016-00025, GINOP-2.3.2-15-2016-00048, GINOP-2.3.2-15-2016-00049, EFOP-3.6.1-16-2016-00004, and ÚNKP-17-4-I-PTE-209 New National Excellence Program of the Ministry of Human Capacities. We thank Anna Pasztor, Laszlo Giran and Janos Schmidt for the technical assistance.

References

[1] M.T. Lin, M.F. Beal, Mitochondrial dysfunction and oxidative stress in neurodegenerative diseases, Nature 443 (7113) (2006) 787–795.
[2] A.H. Schapira, Mitochondrial diseases, Lancet 379 (9828) (2012) 1825–1834.
[3] X. Qiu, L. Cao, X. Yang, X. Zhao, X. Liu, Y. Han, Y. Xue, H. Jiang, Z. Chi, Role of mitochondrial fission in neuronal injury in pilocarpine-induced epileptic rats, Neuroscience 245 (2013) 157–165.
[4] P.A. Andreux, R.H. Houtkooper, J. Auwerx, Pharmacological approaches to restore mitochondrial function, Nat. Rev. Drug Discov. 12 (6) (2013) 465–483.
[5] P.H. Reddy, T.P. Reddy, Mitochondria as a therapeutic target for aging and neurodegenerative diseases, Curr. Alzheimer Res. 8 (4) (2011) 393–409.
[6] P. Belenguer, L. Pellegrini, The dynamin GTPase OPA1: more than mitochondria? Biochim. Biophys. Acta 1833 (1) (2013) 176–183.
[7] M. Liesa, M. Palacin, A. Zorzano, Mitochondrial dynamics in mammalian health and disease, Physiol. Rev. 89 (3) (2009) 799–845.
[8] C.A. Galloway, Y. Yoon, Mitochondrial morphology in metabolic diseases, Antioxidants Redox Signal. 19 (4) (2013) 415–430.
[9] C.M. Nasrallah, T.L. Horvath, Mitochondrial dynamics in the central regulation of metabolism, Nat. Rev. Endocrinol. 10 (11) (2014) 650–658.
[10] D. Gao, S. Nong, X. Huang, Y. Lu, H. Zhao, Y. Lin, Y. Man, S. Wang, J. Yang, J. Li, The effects of palmitate on hepatic insulin resistance are mediated by NADPH Oxidase 3-derived reactive oxygen species through JNK and p38MAPK pathways, J. Biol. Chem. 285 (39) (2010) 29965–29973.

[11] T. Nishikawa, E. Araki, Impact of mitochondrial ROS production in the pathogenesis of diabetes mellitus and its complications, Antioxidants Redox Signal. 9 (3) (2007) 343–353.
[12] N. Houstis, E.D. Rosen, E.S. Lander, Reactive oxygen species have a causal role in multiple forms of insulin resistance, Nature 440 (7086) (2006) 944–948.
[13] W. Song, J. Chen, A. Petrilli, G. Liot, E. Klinglmayr, Y. Zhou, P. Poquiz, J. Tjong, M.A. Pouladi, M.R. Hayden, E. Masliah, M. Ellisman, I. Rouiller, R. Schwarzenbacher, B. Bossy, G. Perkins, E. Bossy-Wetzel, Mutant huntingtin binds the mitochondrial fission GTPase dynamin-related protein-1 and increases its enzymatic activity, Nat. Med. 17 (3) (2011) 377–382.
[14] K. Malpass, Neurodegenerative disease: a novel 3D culture model of tauopathy shows promise as a screening tool for Alzheimer disease therapies, Nat. Rev. Neurol. 9 (1) (2013) 2.
[15] F. Mourkioti, J. Kustan, P. Kraft, J.W. Day, M.M. Zhao, M. Kost-Alimova, A. Protopopov, R.A. DePinho, D. Bernstein, A.K. Meeker, H.M. Blau, Role of telomere dysfunction in cardiac failure in Duchenne muscular dystrophy, Nat. Cell Biol. 15 (8) (2013) 895–904.
[16] J. Giacomotto, N. Brouilly, L. Walter, M.C. Mariol, J. Berger, L. Segalat, T.S. Becker, P.D. Currie, K. Gieseler, Chemical genetics unveils a key role of mitochondrial dynamics, cytochrome c release and IP3R activity in muscular dystrophy, Human Mol. Genet. 22 (22) (2013) 4562–4578.
[17] C.A. Galloway, H. Lee, P.S. Brookes, Y. Yoon, Decreasing mitochondrial fission alleviates hepatic steatosis in a murine model of nonalcoholic fatty liver disease, American journal of physiology, Gastrointest. Liver Physiol. 307 (6) (2014) G632–G641.
[18] H. Pi, S. Xu, L. Zhang, P. Guo, Y. Li, J. Xie, L. Tian, M. He, Y. Lu, M. Li, Y. Zhang, M. Zhong, Y. Xiang, L. Deng, Z. Zhou, Z. Yu, Dynamin 1-like-dependent mitochondrial fission initiates overactive mitophagy in the hepatotoxicity of cadmium, Autophagy 9 (11) (2013) 1780–1800.
[19] S.J. Kim, M. Khan, J. Quan, A. Till, S. Subramani, A. Siddiqui, Hepatitis B virus disrupts mitochondrial dynamics: induces fission and mitophagy to attenuate apoptosis, PLoS Pathogens 9 (12) (2013) e1003722.
[20] D.M. Tabima, S. Frizzell, M.T. Gladwin, Reactive oxygen and nitrogen species in pulmonary hypertension, Free Radical Biol. Med. 52 (9) (2012) 1970–1986.
[21] J. Ryan, A. Dasgupta, J. Huston, K.H. Chen, S.L. Archer, Mitochondrial dynamics in pulmonary arterial hypertension, J. Mol. Med. 93 (3) (2015) 229–242.
[22] J. Marin-Garcia, A.T. Akhmedov, G.W. Moe, Mitochondria in heart failure: the emerging role of mitochondrial dynamics, Heart Failure Rev. 18 (4) (2013) 439–456.
[23] N. Doti, C. Reuther, P.L. Scognamiglio, A.M. Dolga, N. Plesnila, M. Ruvo, C. Culmsee, Inhibition of the AIF/CypA complex protects against intrinsic death pathways induced by oxidative stress, Cell Death Dis. 5 (2014) e993.
[24] S.M. Gehrig, C. van der Poel, T.A. Sayer, J.D. Schertzer, D.C. Henstridge, J.E. Church, S. Lamon, A.P. Russell, K.E. Davies, M.A. Febbraio, G.S. Lynch, Hsp72 preserves muscle function and slows progression of severe muscular dystrophy, Nature 484 (7394) (2012) 394–398.
[25] G. Bardos, K. Moricz, L. Jaszlits, G. Rabloczky, K. Tory, I. Racz, S. Bernath, B. Sumegi, B. Farkas, B. Literati-Nagy, P. Literati-Nagy, BGP-15, a hydroximic acid derivative, protects against cisplatin- or taxol-induced peripheral neuropathy in rats, Toxicol. Appl. Pharmacol. 190 (1) (2003) 9–16.
[26] Z. Sarszegi, E. Bognar, B. Gaszner, A. Konyi, F. Gallyas Jr., B. Sumegi, Z. Berente, BGP-15, a PARP-inhibitor, prevents imatinib-induced cardiotoxicity by activating Akt and suppressing JNK and p38 MAP kinases, Mol. Cell. Biochem. 365 (1–2) (2012) 129–137.
[27] G. Nagy, A. Szarka, G. Lotz, J. Doczi, L. Wunderlich, A. Kiss, K. Jemnitz, Z. Veres, G. Banhegyi, Z. Schaff, B. Sumegi, J. Mandl, BGP-15 inhibits caspase-independent programmed cell death in acetaminophen-induced liver injury, Toxicol. Appl. Pharmacol. 243 (1) (2010) 96–103.
[28] R. Halmosi, Z. Berente, E. Osz, K. Toth, P. Literati-Nagy, B. Sumegi, Effect of poly (ADP-ribose) polymerase inhibitors on the ischemia-reperfusion-induced oxidative cell damage and mitochondrial metabolism in Langendorff heart perfusion system, Mol. Pharmacol. 59 (6) (2001) 1497–1505.
[29] J. Chung, A.K. Nguyen, D.C. Henstridge, A.G. Holmes, M.H. Chan, J.L. Mesa, G.I. Lancaster, R.J. Southgate, C.R. Bruce, S.J. Duffy, I. Horvath, R. Mestril, M.J. Watt, P.L. Hooper, B.A. Kingwell, L. Vigh, A. Hevener, M.A. Febbraio, HSP72 protects against obesity-induced insulin resistance, Proc. Natl. Acad. Sci. USA 105 (5) (2008) 1739–1744.
[30] B. Literati-Nagy, E. Kulcsar, Z. Literati-Nagy, B. Buday, E. Peterfai, T. Horvath, K. Tory, A. Kolonics, A. Fleming, J. Mandl, L. Koranyi, Improvement of insulin sensitivity by a novel drug, BGP-15, in insulin-resistant patients: a proof of concept randomized double-blind clinical trial, Hormone and metabolic research = Hormon- und Stoffwechselforschung = Hormones et metabolisme 41(5) (2009) 374–380.
[31] Z. Literati-Nagy, K. Tory, B. Literati-Nagy, A. Kolonics, L. Vigh Jr., L. Vigh, J. Mandl, Z. Szilvassy, A novel insulin sensitizer drug candidate-BGP-15-can prevent metabolic side effects of atypical antipsychotics, Pathol. Oncol. Res.: POR 18 (4) (2012) 1071–1076.
[32] G. Sapra, Y.K. Tham, N. Cemerlang, A. Matsumoto, H. Kiriazis, B.C. Bernardo, D.C. Henstridge, J.Y. Ooi, L. Pretorius, E.J. Boey, L. Lim, J. Sadoshima, P.J. Meikle, N.A. Mellet, E.A. Woodcock, S. Marasco, T. Ueyama, X.J. Du, M.A. Febbraio, J.R. McMullen, The small-molecule BGP-15 protects against heart failure and atrial fibrillation in mice, Nat. Commun. 5 (2014) 5705.
[33] D.C. Henstridge, C.R. Bruce, B.G. Drew, K. Tory, A. Kolonics, E. Estevez, J. Chung, N. Watson, T. Gardner, R.S. Lee-Young, T. Connor, M.J. Watt, K. Carpenter, M. Hargreaves, S.L. McGee, A.L. Hevener, M.A. Febbraio, Activating HSP72 in rodent skeletal muscle increases mitochondrial number and oxidative capacity and decreases insulin resistance, Diabetes 63 (6) (2014) 1881–1894.
[34] Y.G. Yoon, C.L. Haug, M.D. Koob, Interspecies mitochondrial fusion between mouse and human mitochondria is rapid and efficient, Mitochondrion 7 (3) (2007) 223–229.
[35] A. del Campo, V. Parra, C. Vasquez-Trincado, T. Gutierrez, P.E. Morales, C. Lopez-Crisosto, R. Bravo-Sagua, M.F. Navarro-Marquez, H.E. Verdejo, A. Contreras-Ferrat, R. Troncoso, M. Chiong, S. Lavandero, Mitochondrial fragmentation impairs insulin-dependent glucose uptake by modulating Akt activity through mitochondrial Ca2+ uptake, Am. J. Physiol. Endocrinol. Metab. 306 (1) (2014) E1–E13.
[36] M. Gulden, A. Jess, J. Kammann, E. Maser, H. Seibert, Cytotoxic potency of H2O2 in cell cultures: impact of cell concentration and exposure time, Free Radical Biol. Med. 49 (8) (2010) 1298–1305.
[37] A. Tapodi, B. Debreceni, K. Hanto, Z. Bognar, I. Wittmann, F. Gallyas Jr., G. Varbiro, B. Sumegi, Pivotal role of Akt activation in mitochondrial protection and cell survival by poly(ADP-ribose)polymerase-1 inhibition in oxidative stress, J. Biol. Chem. 280 (42) (2005) 35767–35775.
[38] K. Kovacs, A. Toth, P. Deres, T. Kalai, K. Hideg, F. Gallyas Jr., B. Sumegi, Critical role of PI3-kinase/Akt activation in the PARP inhibitor induced heart function recovery during ischemia-reperfusion, Biochem. Pharmacol. 71 (4) (2006) 441–452.
[39] K. Sumegi, K. Fekete, C. Antus, B. Debreceni, E. Hocsak, F. Gallyas Jr., B. Sumegi, A. Szabo, BGP-15 protects against oxidative stress- or lipopolysaccharide-induced mitochondrial destabilization and reduces mitochondrial production of reactive oxygen species, PloS one 12 (1) (2017) e0169372.
[40] G. Elachouri, S. Vidoni, C. Zanna, A. Pattyn, H. Boukhaddaoui, K. Gaget, P. Yu-Wai-Man, G. Gasparre, E. Sarzi, C. Delettre, A. Olichon, D. Loiseau, P. Reynier, P.F. Chinnery, A. Rotig, V. Carelli, C.P. Hamel, M. Rugolo, G. Lenaers, OPA1 links human mitochondrial genome maintenance to mtDNA replication and distribution, Genome Res. 21 (1) (2011) 12–20.
[41] H. Lee, S.B. Smith, Y. Yoon, The short variant of the mitochondrial dynamin OPA1 maintains mitochondrial energetics and cristae structure, J. Biol. Chem. 292 (17) (2017) 7115–7130.
[42] N. Xie, C. Wang, Y. Lian, H. Zhang, C. Wu, Q. Zhang, A selective inhibitor of Drp1, mdivi-1, protects against cell death of hippocampal neurons in pilocarpine-induced seizures in rats, Neurosci. Lett. 545 (2013) 64–68.
[43] X. Ma, Y. Xie, Y. Chen, B. Han, J. Li, S. Qi, Post-ischemia mdivi-1 treatment protects against ischemia/reperfusion-induced brain injury in a rat model, Neurosci. Lett. 632 (2016) 23–32.
[44] N. Ishihara, M. Nomura, A. Jofuku, H. Kato, S.O. Suzuki, K. Masuda, H. Otera, Y. Nakanishi, I. Nonaka, Y. Goto, N. Taguchi, H. Morinaga, M. Maeda, R. Takayanagi, S. Yokota, K. Mihara, Mitochondrial fission factor Drp1 is essential for embryonic development and synapse formation in mice, Nat. Cell Biol. 11 (8) (2009) 958–966.
[45] E.A. Bordt, P. Clerc, B.A. Roelofs, A.J. Saladino, L. Tretter, V. Adam-Vizi, E. Cherok, A. Khalil, N. Yadava, S.X. Ge, T.C. Francis, N.W. Kennedy, L.K. Picton, T. Kumar, S. Uppuluri, A.M. Miller, K. Itoh, M. Karbowski, H. Sesaki, R.B. Hill, B.M. Polster, The putative Drp1 inhibitor mdivi-1 Is a reversible mitochondrial complex I inhibitor that modulates reactive oxygen species, Develop. Cell 40(6) (2017) 583–594 e586.
[46] T. Marunouchi, M. Murata, N. Takagi, K. Tanonaka, Possible involvement of phosphorylated heat-shock factor-1 in changes in heat shock protein 72 induction in the failing rat heart following myocardial infarction, Biol. Pharm. Bull. 36 (8) (2013) 1332–1340.